

# Discovery Potential of the Standard Model Higgs Boson Through $H \rightarrow WW$ Decay Mode with the ATLAS Detector at LHC

H.J. Yang (on behalf of the ATLAS Collaboration)

Department of Physics, University of Michigan, Ann Arbor, MI 48109-1120, USA

We report results of a study of the Standard Model Higgs boson discovery potential through the W-pair leptonic decay modes with the ATLAS detector at LHC at 14 TeV center-of-mass energy. We used MC samples with full detector simulation and reconstruction of the ATLAS experiment to estimate the ATLAS detection sensitivity for the reaction of  $pp \rightarrow H \rightarrow WW \rightarrow e\nu\mu\nu$  with no hard jet or two hard jets in the final states. The prospects for the Higgs boson searches at ATLAS are presented, including trigger efficiencies and data-driven methods to estimate the backgrounds using control samples in data. With  $10 \text{ fb}^{-1}$  of integrated luminosity, one would expect to discover a Standard Model Higgs boson with ATLAS detector in Higgs boson mass range  $135 < m_H < 190$  GeV. If the Higgs boson does not exist, we will extend and confirm the exclusion produced by the Tevatron Higgs boson search result, which has ruled out the Higgs boson mass range of  $160 < m_H < 170$  GeV at 95% confidence level. If Higgs boson would be discovered, ATLAS could measure its mass with a precision of about 2 and 7 GeV for Higgs boson mass around 160 GeV and 130 GeV, respectively.

arXiv:0910.0193v1 [hep-ex] 1 Oct 2009

## 1. Introduction

The Standard Model (SM) of particle physics is a successful theory confirmed by numerous measurements since the 1970's. After the direct observations of the massive top quark and the  $\nu_\tau$  at Fermilab in 1995 and 2000, respectively, only one fundamental particle predicted by the SM, the Higgs boson, remains to be discovered. The role of the Higgs boson is critical in the SM because fermions and W/Z bosons, via a process of spontaneous symmetry breaking, acquire their mass through interactions with the Higgs boson fields. In the SM the Higgs boson couplings to all fermions and electroweak gauge bosons depend on their masses. Generically, the SM Higgs boson couples most strongly to heavy particles. However, the SM doesn't predict the Higgs boson mass, which resulted in a great experimental challenging to search for the Higgs boson in a very wide mass range and through many different decay modes.

The Leading Order (LO) SM Higgs boson production mechanism at the LHC (Large Hadron Collider) is shown by the Feynman diagrams in Figure 1, including the processes of the Gluon-Gluon Fusion (GGF), the  $t\bar{t}$  fusion, the Higgs-strahlung and the Vector-Boson Fusion (VBF). The dominant process is the GGF Higgs boson as shown in the next-to-leading-order (NLO) cross-section plot in the Figure 2. Higgs boson production via VBF is also an important production mechanism for Higgs boson searches at the LHC with the specific signature of a Higgs boson with two hard jets in the final states. The Higgs boson production cross-section is very small compared to the enormous QCD jet productions at the LHC. The ability to detect and identify the Higgs boson decay final states (see Figure 3) [1] is crucial to the success of the Higgs boson discovery.

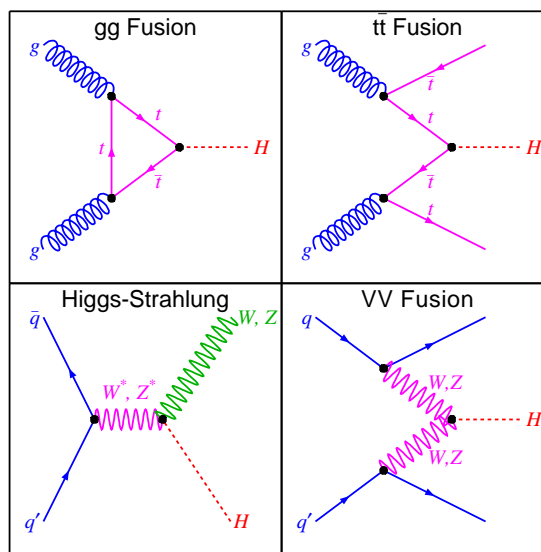


Figure 1: SM Higgs boson production LO Feynman diagrams.

The direct search at LEP sets a lower Higgs boson mass limit of 114.4 GeV at 95% confidence level [2]. Recent searches at Tevatron exclude the Higgs boson mass between 160 GeV and 170 GeV at 95% confidence level [3]. The electroweak data constraints deduced from consistency conditions of the SM can be used to derive an upper limit of SM Higgs boson mass of 190 GeV at 95% C.L.[1, 4]. Therefore the most interesting mass range indicated by direct Higgs boson search and indirect constraints is between 114 GeV and 190 GeV.

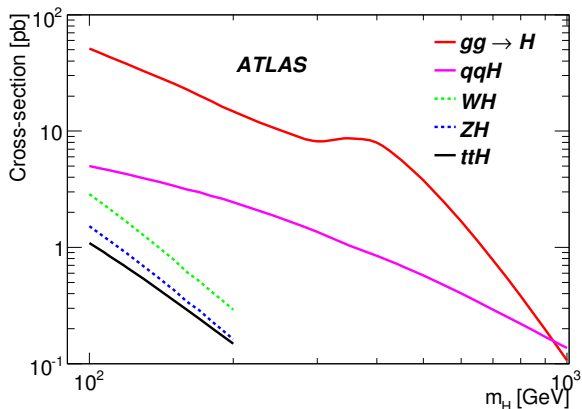


Figure 2: SM Higgs boson production NLO cross-sections at the LHC at 14 TeV

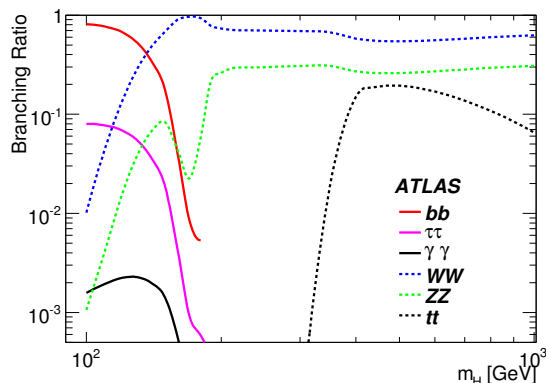


Figure 3: SM Higgs boson decay branching ratios

## 2. Monte Carlo Samples

As shown in the Figure 2, there are two dominant Higgs boson production modes: GGF and VBF, which are in the kinematic region of interest for the  $H \rightarrow WW$  decay mode. When both W bosons decay to leptons, the Higgs boson signature includes two energetic leptons with large missing transverse energy in the final state. These two leptons tend to go same direction due to spin correlation. For the VBF Higgs boson, the final state also includes two hard jets which tend to be well-separated in pseudo-rapidity. The Higgs boson signal and major background sources (SM  $WW$ ,  $t\bar{t}$ , Z+jets and W+jets) are listed in Table I. The MC generators we used to produce MC events and corresponding cross sections are also listed in the Table I.

Table I Monte Carlo generators and cross sections for the Higgs boson signal and background processes. The W+jets cross sections listed is the cross section per lepton flavor.

Physics Process	Generator	$\sigma(\text{pb})$
$gg \rightarrow H \rightarrow WW (M_H = 170 \text{ GeV})$	MC@NLO	19.418
VBF $H \rightarrow WW (M_H = 170 \text{ GeV})$	Pythia	2.853
$qq/qq \rightarrow WW$	MC@NLO	111.6
$gg \rightarrow WW$	GG2WW	5.26
$pp \rightarrow t\bar{t}$	MC@NLO	833.0
$Z \rightarrow \tau\tau + \text{jets}$	ALPGEN	2015
$W \rightarrow \ell\nu + \text{jets}$	ALPGEN	20510

## 3. Leptonic W Pair Production with No Hard Jets

The event selection for  $H \rightarrow WW \rightarrow \ell\nu\ell\nu$  channel consists of a set of simple cuts.

- Require that the selected event has exactly two isolated, opposite-charge leptons (electron or muon) with  $P_T > 15 \text{ GeV}$ .
- To suppress single-top background, backgrounds from dileptonic decays of  $b\bar{b}$  and  $c\bar{c}$  resonances, and lepton pairs from  $b \rightarrow c$  cascade decays, require that the invariant mass  $m_{\ell\ell}$  of the leptons is between 12 GeV and 300 GeV.
- Require that the event has missing transverse energy  $E_T^{miss} > 30 \text{ GeV}$ .
- To suppress  $Z \rightarrow \tau\tau$  background, reject events which have invariant mass of a hypothetical  $\tau$  pair in the range  $|M_{\tau\tau} - M_Z| < 25 \text{ GeV}$ .
- To suppress backgrounds from top quark decays, reject events that contain any hard jets with  $p_T > 20 \text{ GeV}$  and  $|\eta_j| < 4.8$ .
- To further suppress the top-related background, reject events with any jets with  $p_T > 15 \text{ GeV}$  and a b-tagging weight greater than 4.

Table II shows the cross sections in the  $e\mu$  channel for signal and background after these cuts.

Events are required to pass at least one of the ATLAS single-lepton or double-lepton triggers [1]. The following notation is used to label different trigger items: e (electron), EM (electromagnetic), MU or mu (muon), I or i (isolated). As an example 2EM15I means two isolated electromagnetic objects with transverse energy  $E_T > 15 \text{ GeV}$ . The Level-1 (L1) trigger menus used here are 2EM15I, EM25I,

Table II Cut flows(in fb) for  $M_H = 170$  GeV in the  $H + 0j, H \rightarrow WW \rightarrow e\nu\mu\nu$  channel. The WW background contains the two processes  $q\bar{q} \rightarrow WW$  and  $gg \rightarrow WW$ .

Selection	Selection Cuts	$gg \rightarrow H$	$t\bar{t}$	WW	$Z \rightarrow \tau\tau$	W+jets
Pre-selection	Lepton Selection + $M_{\ell\ell}$	166.4	6501	718.12	4171	209.1
	$E_T^{miss} > 30$ GeV	147.7	5617	505.25	526.3	181.6
	$Z \rightarrow \tau\tau$ Rejection	145.8	5215	485.12	164.2	150.4
	Jet Veto	61.80	14.84	238.35	31.91	76.12
	b-veto	61.56	6.85	237.87	30.76	76.12
Signal region	$\Delta\phi < 1.575, M_T < 600$ GeV	$50.6 \pm 2.5$	$2.3 \pm 1.6$	$85.4 \pm 2.7$	$< 1.7$	$38 \pm 38$
Control region	$\Delta\phi > 1.575, M_T < 600$ GeV	$10.9 \pm 1.1$	$4.6 \pm 2.3$	$151.9 \pm 3.6$	$30.8 \pm 4.2$	$38 \pm 38$

EM60I, MU20 and MU40. For the Level-2 (L2) trigger and Event Filter (EF), events are required to pass the e25i, 2e15i, e60 or mu20i triggers. For the  $e\mu$  channel, the trigger efficiency for L1 is 99.0%; for L2 it is 96.7%, and for EF it is 95.2%. The trigger efficiency for signal is quite high and the trigger efficiency does not distort the shapes of the kinematic variables of interest in the signal in a significant way. Table II does not include the trigger efficiency.

After the basic event selection, the signal to background ratio is about 1:4. This analysis focuses on three variables:

- the transverse opening angle  $\Delta\phi_{\ell\ell}$ ; a cut on this variable exploits differences in the spin correlations in the WW system in the Higgs boson signal and the WW background (Figure 4).
- the transverse momentum of the WW system,  $p_T^{WW}$ , which tends to be slightly larger for signal than for WW background because gluon-initiated processes tend to have more initial-state radiation than quark-initiated processes (Figure 5).
- the transverse mass which is defined as  $M_T = \sqrt{(E_T^{\ell\ell} + E_T^{miss})^2 - (p_T^{\ell\ell} + p_T^{miss})^2}$  (Figure 6).

### 3.1. Fitting Algorithm

A 2-dimensional fit of transverse mass ( $M_T$ ) and  $p_T^{WW}$  in two bins of the dilepton opening angle  $\Delta\phi_{\ell\ell}$  in the transverse plane has been implemented. After the preselection cuts and the additional requirement that  $M_T < 600$  GeV is applied, the remaining events are separated into two subsamples, one with  $\Delta\phi_{\ell\ell} < 1.575$  (signal region) and the other with  $\Delta\phi_{\ell\ell} > 1.575$  (control region), as listed in Table II.

The top background is estimated with the help of b-tagged control samples with the same kinematic

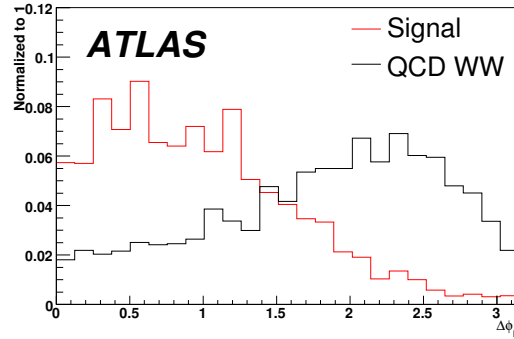


Figure 4: Transverse opening angle  $\Delta\phi_{\ell\ell}$  of two leptons after preselection cuts.

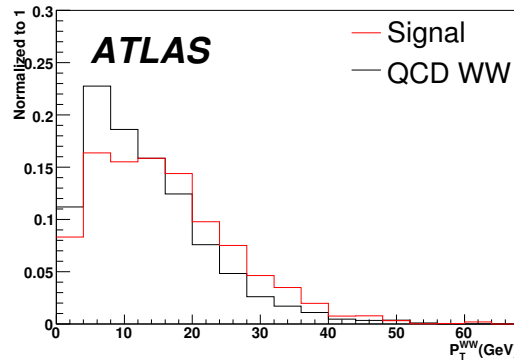


Figure 5: Transverse momentum  $p_T^{WW}$  of the WW system after preselection cuts.

cuts as the signal-enriched and background-enriched regions. The  $t\bar{t}$  cross section is estimated based on Monte Carlo samples that use MC@NLO to model the top background. Standalone fits are performed on the b-tagged control samples before the fit to the b-vetoed regions begins, the top background in the b-

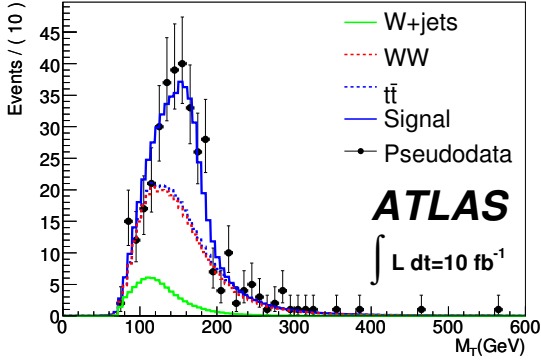


Figure 6: Transverse mass  $M_T$  for events with  $\Delta\phi_{\ell\ell} < 1.575$  and  $p_T^{WW} > 20$  GeV assuming a SM Higgs boson with  $M_H = 170$  GeV and  $10 \text{ fb}^{-1}$  integrated luminosity.

vetoed regions is estimated by extrapolating both the shape and the normalization from the b-tagged region to the b-vetoed region based on ratios obtained from MC@NLO.

The  $Z \rightarrow \tau\tau$  background is normalized and its shape is determined by studying a sample of  $Z \rightarrow \mu\mu$  events taken from real data, where the reconstructed muons are replaced by simulated taus. Two muon events with a dimuon invariant mass between 82 and 98 GeV are selected, and the same jet veto is applied to selected events. After event selection cuts are applied, the effective cross section of  $Z \rightarrow \tau\tau$  background is about 250 fb. A standalone fit to these “data-Monte-Carlo” events is performed to determine the shape and normalization of the  $Z \rightarrow \tau\tau$  background; in the final fit, the shape parameters obtained from the fit to control sample are fixed and the normalization is rescaled by a factor that is assumed in this study to be well-predicted.

W+jets is one of the main sources of fake backgrounds for the dilepton channels, it is crucial to achieve a good rejection against this background. The average jet fake as electron rate is  $(1.7 \pm 0.2) \times 10^{-4}$  before isolation and  $(6.7 \pm 1.5) \times 10^{-5}$  after electron isolation. The corresponding jet fake as muon rate is  $(1.7 \pm 0.6) \times 10^{-5}$  after isolation cuts are applied. For W+jets background estimation, due the limited size of the available W+jets Monte Carlo sample, the shape of the transverse mass and  $p_T^{WW}$  distributions are taken from a set of events with loosen isolation and shower shape cuts. Further detailed studies are needed to estimate W+jets background.

Once the fits to the control samples are completed, a simultaneous fit to the two  $\Delta\phi_{\ell\ell}$  bins in the b-vetoed region is performed. A few of the parameters that described the shape of the transverse mass and  $p_T^{WW}$

distributions of the WW background are allowed to float in the fit. The normalizations of the WW background are free to float independently. However, we add a penalty term of the form  $(R_{fit} - R_{true})/\sigma_R^2$ , where  $R_{fit}$  is the ratio of the best-fit number of WW background events in the small- $\Delta\phi_{\ell\ell}$  region over the number in the large- $\Delta\phi_{\ell\ell}$  region,  $R_{true}$  is the Monte Carlo prediction of the ratio taken from the central-value calculation, and  $\sigma_R$  is the uncertainty in the prediction of  $R_{true}$ , taken to be 10%.

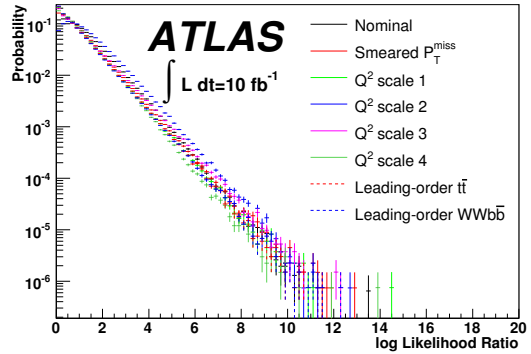


Figure 7: The log Likelihood Ratio distributions for background-only Monte Carlo in  $H + 0j$ ,  $H \rightarrow WW \rightarrow e\nu\mu\nu$  assuming  $10 \text{ fb}^{-1}$ .

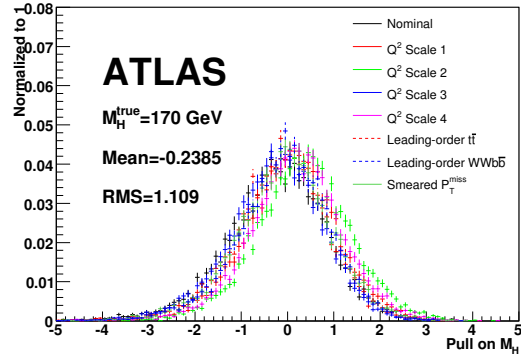


Figure 8: The pull distributions for  $M_H = 170$  GeV for Higgs boson signal and background Monte Carlo in  $H + 0j$ ,  $H \rightarrow WW \rightarrow e\nu\mu\nu$  assuming  $10 \text{ fb}^{-1}$ .

In order to demonstrate the robustness of the fit against systematic uncertainties, top Monte Carlo has been used to compute the sampling distributions for the Likelihood Ratio in several scenarios where the “true” probability distribution has been distorted to model various sources of systematic error. Seven distorted scenarios are considered: four altered  $Q^2$

scale choices (factorization and renormalization scales raised and lowered by factors of 8), two alternative top background models (based on leading-order  $pp \rightarrow WWbb$  and leading-order  $pp \rightarrow tt \rightarrow WWbb$ ), and one alternative model of all irreducible backgrounds where the  $x$  and  $y$  components of  $E_T^{miss}$  have been independently smeared by 5 GeV each. Figure 7 shows the Likelihood Ratio distributions for background-only outcomes and Figure 8 represents the distributions of pulls of the fitted Higgs boson mass for signal plus background with a true Higgs boson mass of 170 GeV.

The linearity of the mass determination as a function of the true Higgs boson mass is shown in Figure 9. The line shows the mean of a Gaussian fit to the region around the peak of the distribution of best-fit Higgs boson masses in the Monte Carlo sample for the case of nominal detector performance. The green band shows the width of the Gaussian fit and is a direct measure of the variability of the mass estimate on repetition of the experiment, the error bars show the median fit error. The typical variability of the mass determinations with  $10 \text{ fb}^{-1}$  integrated luminosity are 5.2 GeV, 1.6 GeV and 4.2 GeV at  $M_H = 130, 160$  and  $190 \text{ GeV}$ , respectively.

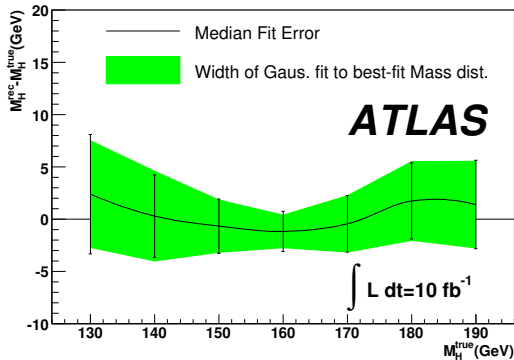


Figure 9: The linearity of the Higgs boson mass determination for  $H + 0j, H \rightarrow WW \rightarrow e\nu\mu\nu$  at  $10 \text{ fb}^{-1}$  integrated luminosity.

The  $H \rightarrow WW \rightarrow e\nu\mu\nu$  is the most promising channel for Higgs boson masses near the  $WW$  threshold. The expected SM Higgs boson detection significance assuming  $10 \text{ fb}^{-1}$  integrated luminosity is shown in Figure 10.

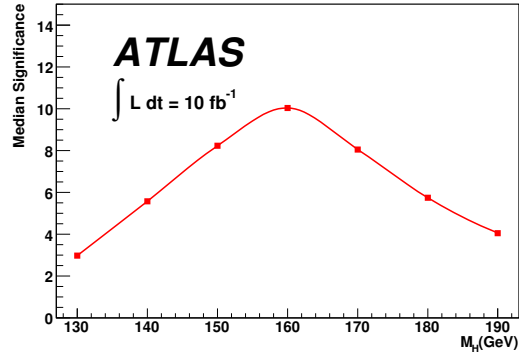


Figure 10: The expected Higgs boson detection significance for the  $H + 0j, H \rightarrow WW \rightarrow e\nu\mu\nu$  at  $10 \text{ fb}^{-1}$  integrated luminosity.

#### 4. Leptonic W Pair Production with Two Hard Jets

For SM Higgs boson produced through VBF production mechanism, the final state has two energetic leptons from both W bosons leptonic decays associated with two hard jets. The distinctive characteristics of VBF Higgs boson signal include:

- The two jets arising from struck quarks tend to be the highest- $p_T$  jets in the events, and they tend to be well-separated in pseudo-rapidity;
- they tend to have a large invariant mass;
- there is very little jet activity in the region between the two tagging jets.

Figure 11 shows the distribution of the pseudo-rapidity gap between two tagging jets (top left), invariant mass of two tagging jets (top right), azimuthal angle between two tagging jets (bottom left) and transverse energy of the third jet (bottom right). Where black solid histograms represent VBF Higgs boson signal with  $M_H = 170 \text{ GeV}$ , green dash-dotted histograms mean  $WW$  background, red dotted histograms are  $t\bar{t}$  and blue dashed histograms are  $Z$ +jets background.

The following cuts have been applied to selected  $H + 2j, H \rightarrow WW \rightarrow \ell\nu\ell\nu$  events.

- Two isolated leptons with  $p_T > 15 \text{ GeV}$
- Missing transverse energy  $E_T^{miss} > 30 \text{ GeV}$
- At least two jets with  $p_T > 20 \text{ GeV}$  and  $|\eta| < 4.8$
- The two jets with highest transverse momentum are required to be in opposite hemispheres with  $\Delta\eta(jet1, jet2) > 3$

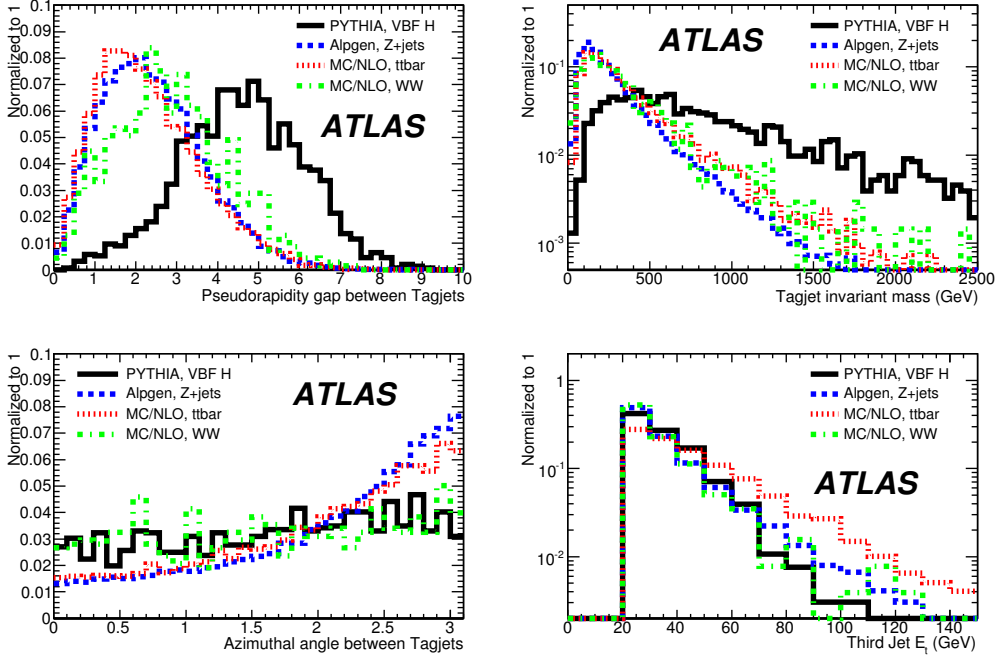


Figure 11: Pseudo-rapidity gap between two tagging jets(top left), invariant mass distribution of two tagging jets(top right), azimuthal angle gap between two tagging jets(bottom left) and  $E_T$  of the third jet(bottom right).

Table III Cut flows(in fb) for  $M_H = 170$  GeV in the  $H + 2j, H \rightarrow WW \rightarrow e\nu\mu\nu$  channel.

Selection Cuts	VBF H (170 GeV)	$t\bar{t}$	WW+jets	$Z \rightarrow \tau\tau$	W+jets
Lepton Selection	30.20	8317	838.96	2096	1323
Forward Jet Tagging	17.27	946.6	32.77	79.3	31.83
Leptons Between Jets	16.47	617.8	22.92	55.13	27.91
$Z \rightarrow \tau\tau$ Rejection	15.68	561.8	21.20	39.03	27.91
$E_T^{miss}, M_T, m_T^{\ell\nu}$	12.78	425.9	15.28	0	13.96
b-veto	12.67	206.72	-	-	-
signal box, b-jet veto	$9.28 \pm 0.27$	$28.5 \pm 5.7$	$4.75 \pm 0.30$	-	$4.3 \pm 4.3$
signal box, no b-jet veto	9.65	114.2	4.99	-	6.07
Control box, b-jet veto	$3.02 \pm 0.15$	$89 \pm 10$	$9.78 \pm 0.43$	-	$7.9 \pm 5.0$
Control box, no b-jet veto	3.13	311.7	10.28	-	7.89

- Require that both leptons are between the two leading jets in pseudo-rapidity
- Reject event which has  $|M_{\tau\tau} - M_Z| < 25$  GeV
- Require transverse mass  $50 < M_T < 600$  GeV
- Require transverse mass  $m_T^{\ell\nu} > 30$  GeV,  $m_T^{\ell\nu} = \sqrt{2P_T(\ell)P_T^{miss} \cdot (1 - \cos\Delta\phi)}$  where  $\Delta\phi$  is the angle between the di-lepton vector and the  $P_T^{miss}$  vector in the transverse plane.

- To suppress b-related background, b-veto cuts are applied on both tagging jets

Table III shows the cut flows (in fb) for  $M_H = 170$  GeV in the  $H + 2j, H \rightarrow WW \rightarrow e\nu\mu\nu$  channel. If the event has  $\Delta\phi_{\ell\ell} < 1.5$  and  $\Delta\eta_{\ell\ell} < 1.4$ , it lies in the signal box; otherwise, it lies in the control region. The trigger efficiency of 99.0% after Level 1, 96.8% after Level 2, and 94.5% after the Event Filter.

After the preselection, a four-variable Neural Network is used to further enhance the separation be-

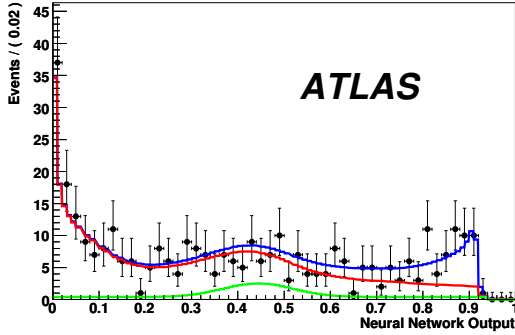


Figure 12: The Neural Network output distribution in the signal box, for the 170 GeV  $H + 2j$ ,  $H \rightarrow WW \rightarrow e\nu\mu\nu$  at  $10 \text{ fb}^{-1}$  integrated luminosity.

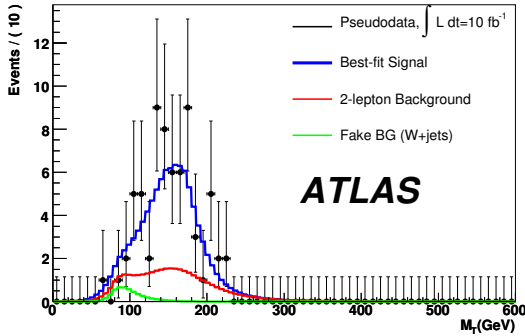


Figure 13: The transverse mass distribution for events in the signal box with Neural Network output larger than 0.8 for the 170 GeV  $H + 2j$ ,  $H \rightarrow WW \rightarrow e\nu\mu\nu$  at  $10 \text{ fb}^{-1}$  integrated luminosity.

tween the signal and the background. The inputs to the Neural Network are:

- $\Delta\eta(\text{jet1}, \text{jet2})$ , the pseudo-rapidity gap between two tagging jets
- $M_{jj}$ , the invariant mass of two tagging jets
- the transverse momentum of the leading non-tagging jet in the region  $|\eta| < 3.2$
- $\eta^* = \eta_3 - (\eta_1 + \eta_2)/2$ , the pseudo-rapidity gap between two tagging jets and the third non-tagging jet.

The Neural Network output distribution in the signal box is shown in Figure 12. The transverse mass distribution for events in the signal box with Neural Network output larger than 0.8 is shown in Figure 13, where black dots with error bar show Pseudodata, blue curve shows best-fit Higgs boson signal, red

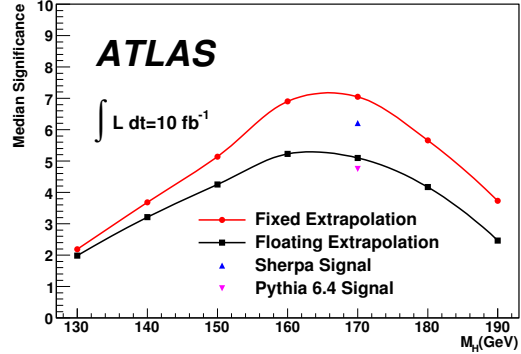


Figure 14: The expected Higgs boson detection significance for the  $H + 2j$ ,  $H \rightarrow WW \rightarrow e\nu\mu\nu$  at  $10 \text{ fb}^{-1}$  integrated luminosity.

curve represents 2-lepton background and green curve is faked background from  $W + \text{jets}$ .

The fit is a two-dimensional fit to the Neural Network output and transverse mass distributions. Both the signal model and the background model are uncorrelated product probability density functions (PDFs). The Neural Network output distribution for the background in the signal box is taken to be the same as the distribution in the control region, but it is multiplied by a linear extrapolation factor. Apart from the slope of this extrapolation factor, all parameters governing the shape of the Neural Network output distribution in the two regions are required to be the same. The expected significance is shown as a function of the true Higgs boson mass in Figure 14.

## 5. Further Improvements

We expect further improvements for Higgs boson detection sensitivity. The analysis presented above only includes the  $e\nu\mu\nu$  channel with jet-veto or two forward jet tagging in events. Including the  $e\nu e\nu$  and  $\mu\nu\mu\nu$  channels and adding dilepton events with 1 jet in final states will certainly increase the detection sensitivity in ATLAS. Based on LEP and Tevatron Higgs boson search experiences, the analysis can be carried out by using multivariate techniques, such as Artificial Neural Networks (ANN) and Boosted Decision Trees (BDT) [5], which would further improve the detection sensitivities. ATLAS physics group has extensively explored these advanced analysis methods [1] and fully developed the tools that will be used in Higgs boson search program with LHC collision data.

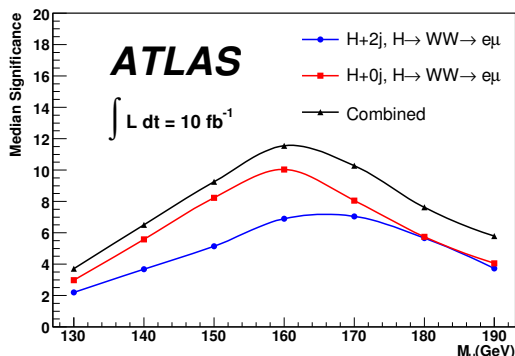


Figure 15: The expected Higgs boson detection significance for the  $H + 0j$  and  $H + 2j$ ,  $H \rightarrow WW \rightarrow e\nu\mu\nu$  at  $10 \text{ fb}^{-1}$  integrated luminosity.

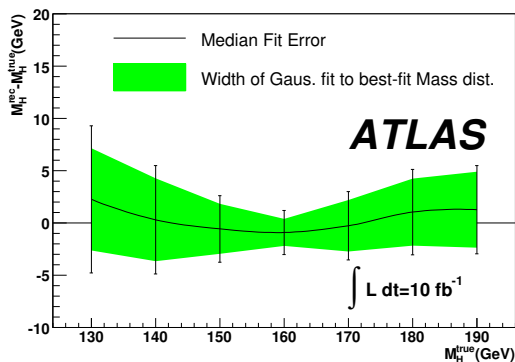


Figure 16: The linearity of the mass determination for the combined fit of  $H + 0/2j$ ,  $H \rightarrow WW \rightarrow e\nu\mu\nu$  at  $10 \text{ fb}^{-1}$  integrated luminosity.

## 6. Conclusions

The prospects for SM Higgs boson searches in the  $WW$  decay mode have been studied using a realistic model of the ATLAS detector. The  $H + 0j$ ,  $H \rightarrow WW \rightarrow e\nu\mu\nu$  channel is very promising for Higgs boson masses in the region around the  $WW$  threshold. With  $10 \text{ fb}^{-1}$  of integrated luminosity, one would expect to be able to achieve a  $5\sigma$  discovery with the  $H \rightarrow WW \rightarrow e\nu\mu\nu$  channel alone if there a SM Higgs boson with a mass between  $\sim 140 \text{ GeV}$  and  $\sim 185 \text{ GeV}$ . A measurement of the mass of the Higgs

boson at  $10 \text{ fb}^{-1}$  integrated luminosity would have a precision of less than  $2 \text{ GeV}$  for Higgs mass boson of  $160 \text{ GeV}$ , or a precision of less than  $4 \text{ GeV}$  for Higgs boson with mass of  $140 \text{ GeV}$ . The  $H + 2j$ ,  $H \rightarrow WW \rightarrow e\nu\mu\nu$  channel has a smaller event rate than the  $H + 0j$  channel. With  $10 \text{ fb}^{-1}$  of integrated luminosity, we expect to reach  $5\sigma$  discovery if SM Higgs boson mass between  $150 \text{ GeV}$  and  $180 \text{ GeV}$ . The combined mass determination for the combined fit of  $H + 0/2j$  is shown in Figure 16. The corresponding combined significance as a function of Higgs boson mass is shown in Figure 15.

## Acknowledgments

The author would like to express gratitude to the ATLAS Collaboration for excellent work on the Monte Carlo simulation and the software package for physics analysis. The ATLAS Higgs working group deserves a special thank for producing the results presented in this paper. The author is supported by the Department of Energy (DE-FG02-95ER40899) of the United States.

## References

- [1] ATLAS Collaboration (G. Aad et.al.), *Expected Performance of the ATLAS Experiment - Detector, Trigger and Physics*, CERN-OPEN-2008-020, Geneva, 2008; [arXiv:0901.0512].  
The Trigger for Early Running, p550
- [2] LEP Higgs Working Group, R. Barate et.al., *Search for the standard model higgs boson at LEP*, Phys. Lett. B565 (2003) 61-75.
- [3] CDF and D0 Collaboration, *Combined CDF and D0 Upper Limits on Standard Model Higgs-Boson Production with up to  $4.2 \text{ fb}^{-1}$  of Data*, Fermilab-PUB-09-060-E (2009), [arXiv:0903.4001].
- [4] CMS Collaboration, S. Abdullin et.al., *Summary of the CMS potential for the Higgs boson discovery*, Eur. Phys. J. C 39S2 (2005) 41-61.
- [5] H.J. Yang et.al., Nucl. Instrum. Meth. A555 (2005) 370-385. Nucl. Instrum. Meth. A543 (2005) 577-584, Nucl. Instrum. Meth. A574 (2007) 342-349 JINST 3:P04004 (2008).